Analytical calculation of plasmonic resonances in metal nanoparticles
A simple guide

Locarno, Marco; Brinks, Daan

DOI
10.1119/5.0094967

Publication date
2023

Document Version
Final published version

Published in
American Journal of Physics

JULY 01 2023

Analytical calculation of plasmonic resonances in metal nanoparticles: A simple guide

Marco Locarno ; Daan Brinks

American Journal of Physics 91, 538 (2023)
https://doi.org/10.1119/5.0094967

Analytical calculation of plasmonic resonances in metal nanoparticles: A simple guide

Marco Locarno[a] and Daan Brinks[b]
Department of Imaging Physics, Delft University of Technology, Lorentzweg 1, 2628 CJ Delft, The Netherlands

(Received 7 April 2022; accepted 18 April 2023)

Localized surface plasmons (LSPs) in metal particles are used in medical, chemical, physical, and biological sensing applications. In this paper, we revisit the classical description of LSPs. We use the Drude model and the Quasi-Static approximation to describe the plasmon resonances in terms of the material and the size of the particles embedded in a dielectric host. We then incorporate the Clausius–Mossotti relation to include shape effects in the classical description. Finally, we incorporate surface damping and retardation effects to arrive at a unified, classical description providing an intuitive and realistic model of plasmonic resonances in metal particles. https://doi.org/10.1119/5.0094967

I. INTRODUCTION

Advances in nanotechnology and photonics go hand in hand, from super-resolution microscopy helping us visualize life at the nanoscale,[1] to extreme-UV lithography enabling the creation of nanoscale chips needed to analyze it.[2] At the intersection of photonics and nanotechnology lies the topic of plasmonics.[3] Plasmonics involves the creation, study, and manipulation of signals embedded in optical-frequency oscillations of surface electrons along metal-dielectric interfaces. Plasmonics confines optical-frequency signals to subwavelength-size volumes, thereby providing the interface between optical electromagnetic fields and nanoscopic devices and circuitry.

When an electromagnetic field interacts with a metal nanoparticle, it will lead to charge oscillations in the metal. These collective oscillations, known as plasmons, are excited when the frequency of the electromagnetic field matches the resonant frequency of the metal nanoparticle. The electrons are free to move within the boundaries of the particle but are ultimately confined to its surface. For these reasons, the effect is called a localized surface plasmon (LSP). Given that the oscillation is at the same frequency as the incoming field, the effect is interchangeably called plasmonic resonance.

Designing metal nanoparticles to answer questions in nanophysics, nanochemistry, and nanobiology requires understanding the plasmonic resonance. Due to quantum mechanical effects, the properties of nanoscale objects often cannot be explained intuitively. Fortunately, the most prominent plasmonic effects can be explained within a classical framework. We will begin with a historical perspective. Then, to model the plasmonic resonance in metal nanoparticles, we will need a framework to describe three distinct features: the metallic characteristic, the size (the "nano"), and the shape of the particle. We will introduce the Drude model, a reasonable description of electrons in metals. The quasi-static approximation will then let us take into account the nanoscale size of the particles. Additionally, the generalization of the Clausius–Mossotti relation will let us consider a particle embedded in a dielectric medium and the effect of its shape. By combining these aspects, we are able to build a classical model for the plasmonic resonance in metal nanoparticles. We will then deal with some of the limitations of the quasi-static approximation by introducing final corrections to the model, to extend its validity as far as possible. As our assumptions are all based on classical electromagnetism, the final model will be classical too.

II. BRIEF HISTORY OF PLASMONICS

While nanotechnology emerged as a field only a few decades ago, peculiar optical phenomena due to nanoparticles have intrigued humankind since ancient times. Witnessing and harnessing such "technologies" far preceded any possible scientific explanation: photonic crystals shape light, thus creating spectacular iridescent colors in butterflies,[4] lead-based quantum dots have been involved in black hair dyes manufactured by ancient Greeks and Romans,[5] and copper nanoparticles were employed in red opaque glass production in Egypt and Mesopotamia.[6]

One of the most impressive pieces of glasswork incorporating metal nanoparticles is the Lycurgus cup (Figs. 1(a) and 1(b)). Dated around the 4th century, this Roman cage cup is made up of dichroic glass, so that an observer sees it red if light passes through it, but green if light is reflected to them. Recent analysis showed that the dichroism is due to the presence of colloidal gold and silver nanoparticles dispersed throughout the glass. The embedded particles have diameters around 70 nm, meaning that they are invisible to optical microscopy and require transmission electron microscopy (TEM) to be seen.[7]

Michael Faraday is credited with performing the first scientific experiments on the optical properties of nanoparticles, focusing on gold colloids in the 1850s. He was puzzled by the ruby red color of the solutions he synthesized (Fig. 1(c)), far removed from the aureate color of bulk gold. A satisfying classical explanation of this phenomenon came only in 1904, when Maxwell Garnett combined the new Drude theory of metals with Lord Rayleigh's description of electromagnetic properties of small spheres.[8] Shortly after, in 1912, Richard Gans successfully extended the description of optical phenomena to oblate and prolate spheroids.[9] However, these theories were all purely based on the optical properties of bulk metals, and it was not until 1970 that they were modified by Uwe Kreibig and Peter Zacharias to take their nanoscale size into account.[10] For the first time, they explained the electronic and optical response of silver and gold nanoparticles

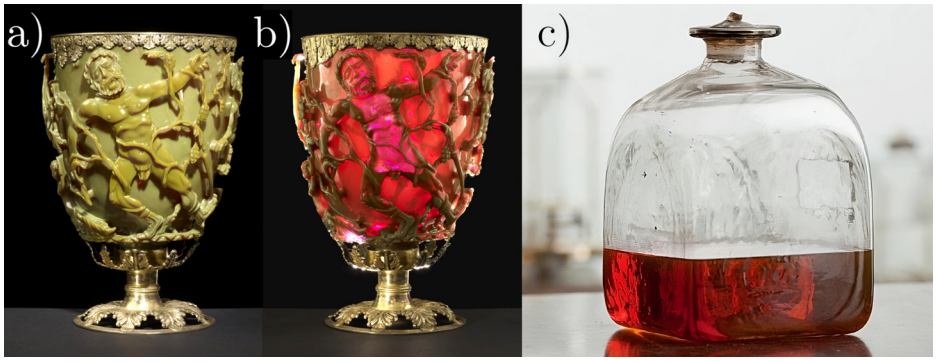

Fig. 1. (Color online) The Lycurgus cup changes color depending whether the light is (a) reflected or (b) transmitted (credits: copyright The Trustees of the British Museum). (c) Faraday's colloidal gold in a glass flask (credits: copyright Paul Wilkinson).

in terms of localized surface plasmon excitations. It became clear then that size, shape, arrangement, medium, and temperature all have a crucial role in controlling the intensity and frequency of plasmonic resonances.

From the early 2000s on, the interest in plasmonics boomed, thanks to novel nanofabrication techniques, commercialization of simulation software and the plethora of biological and biomedical applications.[11,12] To summarize 50 years of research and more than a century of theoretical modeling, we start by examining the object under study, the metal nanoparticle, and its defining features.

III. CLASSICAL DERIVATION OF PLASMONIC RESONANCE

A. Drude model for metals

The electric properties of materials are characterized by the dielectric constant ϵ, which relates the electric displacement $\vec{D}$ to the electric field $\vec{E}$ through the equation $\vec{D} = \epsilon_0\vec{E} + \vec{P} = \epsilon_0\epsilon\vec{E}$. When the applied field is sinusoidal, the dielectric constant is a complex number; the imaginary part represents the out-of-phase response of the material. Within the Drude model, the complex dielectric function of a metal is given by

$$\epsilon_m(\omega) = 1 - \frac{\omega_P^2}{\omega^2 + \gamma^2} - i\frac{\omega_P^2\gamma}{\omega^3 + \gamma^2\omega}. \tag{1}$$

Two derivations of this well-known formula can be found in the supplementary material.[43] Here, $\omega_P = \sqrt{Ne^2/\epsilon_0 m}$ is the plasma frequency and γ is the damping frequency, both dependent on the metal considered. The plasma frequency depends on the carrier density, N, the electron charge, e, and the effective mass of the electron, m. The damping frequency γ is given by Matthiessen's rule for different independent collision events, each possessing a time constant τ_j,

$$\gamma = \sum_j 1/\tau_j. \tag{2}$$

This equation provides the statistical rate at which the electron motion in the bulk material is disrupted due to collisions between electrons and nuclei, defects, impurities, or other electrons. Furthermore, an extension to the Drude model has been formulated to account for the positive background of ions in the constant term $\epsilon_{m,\infty}$, referred to as the core polarization[3,13]

$$\epsilon_m(\omega) = \epsilon_{m,\infty} - \frac{\omega_P^2}{\omega^2 + \gamma^2} - i\frac{\omega_P^2\gamma}{\omega^3 + \gamma^2\omega}. \tag{3}$$

In Table I, we report the Drude parameters for common plasmonic metals, fitted from experimental data in Ref. 14. Note that the experimental and fitted data do not match completely, as the Drude model is an approximation of the actual complex dielectric function, which can include interband and intraband transitions. Throughout the paper, we will take gold as a typical metal for plasmonics.

With these concepts in hand, we can provide a simple yet rigorous derivation of plasmonic resonance in metal nanoparticles.

Table I. Drude parameters for common (bulk) metals.

	$\epsilon_{m,\infty}$	ω_P [rad/s]	γ [rad/s]
Au	7.926	1.23×10^{16}	3.8×10^{13}
Ag	5.303	1.42×10^{16}	1.0×10^{14}
Cu	6.087	1.34×10^{16}	1.5×10^{14}
Al	1	1.93×10^{16}	2.4×10^{14}

B. Quasi-static approximation

If a nanoparticle is much smaller than the wavelength (Fig. 2), then all the electrons inside the nanoparticle feel the same electric field and oscillate in phase. This approach is

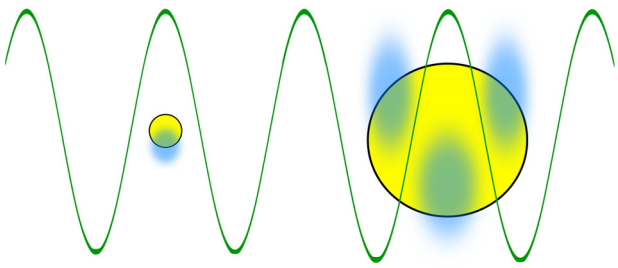

Fig. 2. Dipolar (left) and multipolar (right) excitation of the free electrons in metal nanoparticles. The electron clouds are represented as light blue halos, while the metal cores as solid yellow.

called the quasi-static approximation (QSA). Let d be the size of the nanoparticle, λ the wavelength, $\vec{k}$ the wave vector, ω the angular frequency of the incoming field $\vec{E}^0$, $\vec{r}$ the relative position of an arbitrary point with respect to the center of the nanoparticle, and t the time. If $d \ll \lambda$, then $\vec{k} \cdot \vec{r} \approx 0$ and mathematically we obtain

$$\vec{E}^0(\vec{r}, t) = \vec{E}^0 e^{i(\omega t - \vec{k}\cdot\vec{r})} \approx \vec{E}^0 e^{i\omega t}. \tag{4}$$

Because of this, the polarization is uniform, and the effect of the quasi-static approximation on the total dipole moment of the nanoparticle $\vec{p}_{np}$ is very conveniently translated to

$$\vec{p}_{np} = V\vec{P}, \tag{5}$$

where V is the volume of the nanoparticle and $\vec{P}$ is the polarization density. The quasi-static approximation lets us drop the dependence on the position $\vec{r}$.

The careful reader might point out that the wavelength inside the nanoparticle may not be the same as the one in the dielectric medium. The concept of wavelength itself may even be ill-defined if the field decays exponentially inside the metal. A relevant comparison would then be between the size of the nanoparticle and the skin depth δ of the metal. For common metals like gold, silver, copper, and aluminum, the skin depth at optical frequencies is on the order of a few tens of nanometers. If $d \lesssim \delta$, then the field can penetrate the nanoparticle completely and the uniformity of the polarization can still be assumed. Refer to the supplementary material[43] for more details regarding skin depth.

It is important to note that particles larger than the wavelength may produce a plethora of effects that cannot be explained as the simple radiation of a dipole, due to the occurrence of multipolar effects. Eventually, extremely large particles will exhibit the optical properties of bulk metal.

C. Generalization of the Clausius–Mossotti relation for ellipsoids

Let us now consider an isolated ellipsoid having a complex dielectric function ϵ_m and semiaxes, respectively, a_x, a_y, and a_z, immersed in a dielectric material (from this point on referred to as the "host") having a real and positive dielectric constant ϵ_h (Fig. 3(a)).

The nanoparticle's dipole moment $\vec{p}_{np}$ is a function of its polarizability tensor $\overleftrightarrow{\alpha}$ as well as of the local electric field $\vec{E}_{loc}$. The latter is different from the applied field $\vec{E}^0$ because of the polarization of the host, but if the dielectric medium is linear, homogeneous and isotropic, then the local field will be proportional to the applied field ($\vec{E}_{loc} = \epsilon_h \vec{E}^0$), and so

$$\vec{p}_{np} = \epsilon_0 \overleftrightarrow{\alpha}\, \vec{E}_{loc} = \epsilon_0 \epsilon_h \overleftrightarrow{\alpha}\, \vec{E}^0. \tag{6}$$

To calculate the polarizability, we, therefore, need to find the relation between the dipole moment and the electric field.

First, we notice that the local electric field is the superposition of the applied field and the opposing field produced by the displacement of charges. Although it is a well-known fact that, in the static limit, the electric field in a conductor is zero, we have to consider that under the QSA the order of magnitude of the skin depth is comparable with the size of the nanoparticle. In this case, the local electric field $\vec{E}_{loc}$, defined at the boundary of the nanoparticle, creates a polarization in the metal $\vec{P}_m$; hence electric charges appear at its surface (Fig. 3(b)). As a consequence, the host dielectric also polarizes near the surface ($\vec{P}_h$). We can treat the boundary as an effective medium, encompassing both the charges in the metal and in the host. The effective polarization $\vec{P}$ can be deduced from the difference between the two opposing polarizations. $\vec{P}$ is in the opposite direction from that of the applied field, thus generating a restoring force. The local electric field, for every j-th axis ($j = x, y, z$), is then[15,16]

$$E_{loc,j} = E^0_j - L_j \frac{P_j}{\epsilon_0 \epsilon_h}, \tag{7}$$

where L_j is the depolarization factor which accounts for the shape of the particle itself

$$L_j = \frac{a_x a_y a_z}{2} \int_0^\infty \frac{dq}{(q + a_j^2)\sqrt{\prod_{\eta=x,y,z}(q + a_\eta^2)}}. \tag{8}$$

The depolarization factors arise from the solution of Laplace's equation in ellipsoidal coordinates. A full derivation can be found in Ref. 15.

The effective polarization $\vec{P}$ is the difference of the polarizations of the metal $\vec{P}_m$ and of the host $\vec{P}_h$,[16]

$$\begin{aligned} P_j &= P_{m,j} - P_{h,j} = \epsilon_0 \epsilon_m E_{loc,j} - \epsilon_0 \epsilon_h E_{loc,j} \\ &= \epsilon_0 (\epsilon_m - \epsilon_h) E_{loc,j}. \end{aligned} \tag{9}$$

Combining Eqs. (7) and (9), we write

$$P_j = \epsilon_0 (\epsilon_m - \epsilon_h) \left(E^0_j - L_j \frac{P_j}{\epsilon_0 \epsilon_h} \right). \tag{10}$$

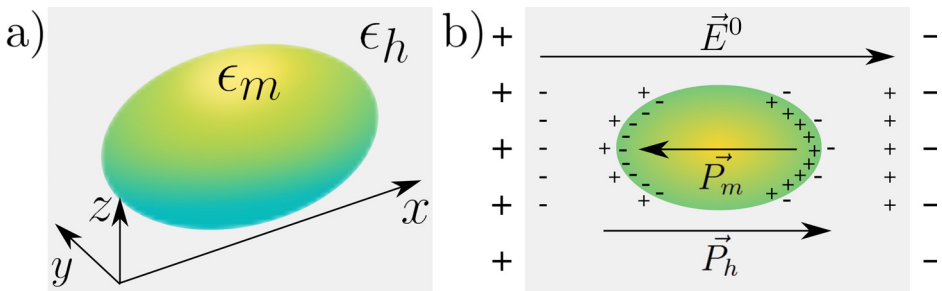

Fig. 3. (a) Ellipsoidal particle immersed in a dielectric medium with the chosen reference system. (b) Snapshot of the incoming electric field and the induced polarization contributions of the metal and the host. This depiction is realistic only in the optical regime and under the quasi-static approximation (QSA), for which the rearrangement of charge is collective and instantaneous.

Solving for P_j,

$$P_j = \frac{\epsilon_0 \epsilon_h (\epsilon_m - \epsilon_h)}{\epsilon_h + L_j(\epsilon_m - \epsilon_h)} E_j^0. \tag{11}$$

Then introducing the quasi-static approximation in Eq. (5) we get

$$p_{np,j} = \epsilon_0 \epsilon_h \underbrace{V \frac{\epsilon_m - \epsilon_h}{\epsilon_h + L_j(\epsilon_m - \epsilon_h)}}_{\alpha_j} E_j^0. \tag{12}$$

Finally, making the volume of the ellipsoid explicit, we obtain the polarizability

$$\alpha_j = \frac{4\pi a_x a_y a_z}{3} \frac{\epsilon_m - \epsilon_h}{\epsilon_h + L_j(\epsilon_m - \epsilon_h)}. \tag{13}$$

It is important to note that $\ddot{\alpha}$ is a diagonal matrix. In other words, if the incoming field is aligned with one of the axes of the ellipsoid, the polarization will be parallel to it. This considerably simplifies the calculations.

Normally, we would have to calculate the integral in Eq. (8), given an arbitrary set of semiaxes lengths. Such calculation is not trivial. Fortunately, an important property of the depolarization factors can drastically simplify the results for simple geometries. The sum of the three depolarization factors is

$$\sum_{j=x,y,z} L_j = 1. \tag{14}$$

A simple, novel proof of this property can be found in the supplementary material.[43]

Thanks to this normalization property, some easy geometries (see Table II) can be treated without calculating the integrals explicitly. Anisotropy is then reflected by the matrix nature of $\ddot{\alpha}$, eventually leading $\vec{p}_{np}$ to not be parallel to $\vec{E}^0$.

The Clausius–Mossotti relation, used to describe the polarizability of spherical particles in a vacuum

$$\alpha_j = 3v \frac{\epsilon_m - 1}{\epsilon_m + 2}, \quad j = x, y, z, \tag{15}$$

in which v is the volume of the spherical particle, coincides with Eq. (13) for $a_x = a_y = a_z$, and $\epsilon_h = 1$. For this reason, Eq. (13) is the generalization of the Clausius–Mossotti relation.

D. Plasmonic resonance

We now have all the tools to calculate the plasmonic resonance. However, what does it mean for a nanoparticle to have a plasmonic resonance? Why do we talk about a plasmonic peak? The simplest way to picture such an effect is by directly plugging the result of the Drude model (Eq. (3)) in the calculation of the polarizability (Eq. (13)). For a sphere with gold-like Drude parameters, put either in vacuum or water, we get the typical wavelength dependence of the polarizability shown in Fig. 4.

The functional form for $|\alpha|$ is a sharp peak. At the angular frequency where the polarizability is maximal, the electrons oscillate with a higher amplitude. Given such a sharp feature in the frequency, we refer to the peak position as the resonance frequency.

To calculate the plasmonic resonance frequency, one can maximize $|\alpha|$. From Eq. (13), it is easy to see that if the denominator approaches zero, the polarizability intensity drastically increases, leading to a strong dipole moment at frequency ω_{res}. This resonance condition translates to the requirement that, in a given direction

$$\mathrm{Re}[\epsilon_m(\omega_{res})] = -\frac{1 - L_j}{L_j}\epsilon_h, \quad \mathrm{Im}[\epsilon_m(\omega_{res})] \approx 0. \tag{16}$$

We see that the resonance frequency depends on the geometrical features of the nanoparticle and on the dielectric medium in which it is immersed. The generalized formula for the resonance frequency ω_{res} for an arbitrary metal nanoparticle can be obtained by combining Eq. (16) with the result of the Drude model (Eq. (3))

$$\omega_{res} = \sqrt{\frac{\omega_P^2}{\epsilon_{m,\infty} + \frac{1 - L_j}{L_j}\epsilon_h} - \gamma^2} \approx \frac{\omega_P}{\sqrt{\epsilon_{m,\infty} + \frac{1 - L_j}{L_j}\epsilon_h}}, \tag{17}$$

where the reasonable assumption of $\omega_P \gg \gamma$ has been introduced (refer to Table I for the realistic orders of magnitude). The shift due to changes in ϵ_h enables a multitude of sensing applications. In the host dielectric environment, variations due to chemical, physical or biological activity result in fact in shifts in plasmonic peaks.[17–19]

In the case of a sphere ($L_j = 1/3, \forall j$), the above equations reduce to the Fröhlich condition

Table II. Depolarization factors for some typical shapes.

Particle shape	Semiaxes	Depolarization factors
Sphere	$a_x = a_y = a_z$	$L_x = L_y = L_z = 1/3$
Long cylinder	$a_x \gg a_y, a_z$	$L_x = 0, \quad L_y = L_z = 1/2$
Large disk	$a_x = a_y \gg a_z$	$L_x = L_y = 0, \quad L_z = 1$

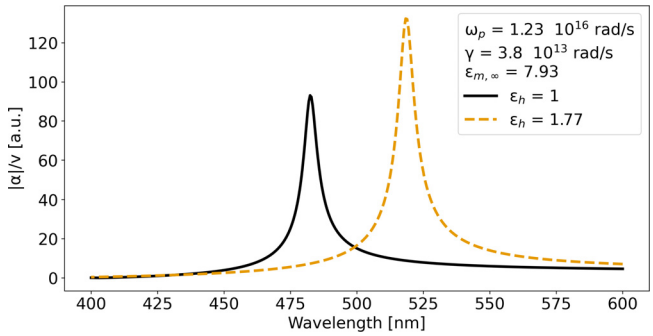

Fig. 4. The volume polarizability of a nanosphere with gold-like parameters, calculated from Eqs. (3) and (13), immersed either in vacuum ($\epsilon_h = 1$) or in water ($\epsilon_h = 1.77$), exhibits a peak in wavelengths. (Plot colors have been selected according to the color-vision deficiency friendly color cycle proposed by Okabe and Ito and made popular by Wong (Ref. 41).)

$$\mathrm{Re}[\epsilon_m(\omega_{res})] = -2\epsilon_h, \quad \mathrm{Im}[\epsilon_m(\omega_{res})] \approx 0,$$
$$\omega_{res} \approx \frac{\omega_P}{\sqrt{\epsilon_{m,\infty} + 2\epsilon_h}}. \tag{18}$$

As expected, Eq. (18) predicts the correct positions[20] for the resonance peak for a nanosphere with gold-like Drude parameters: when in vacuum $\omega_{res} \approx 3.9 \times 10^{15}$ rad/s ($\lambda_{res} \approx 480$ nm), while when in water $\omega_{res} \approx 3.6 \times 10^{15}$ rad/s ($\lambda_{res} \approx 520$ nm). This surprisingly simple result is already sufficient to explain the color of Faraday's colloidal gold (Fig. 1(c)). As the solution contains gold nanospheres, the resonance frequency ω_{res} will be in the cyan-green part of the spectrum, so it appears ruby red when illuminated by white light.

Unfortunately, only a few materials satisfy Eq. (18) in the optical range. For the resonance to exist, the imaginary part of the dielectric function must be sufficiently low. For this reason, the most significant plasmonic materials are also the most conductive: silver, gold, copper, and aluminum. Other less commonly used metals are palladium, platinum and nickel.[21] An invaluable contribution to the investigation of plasmonic candidates was given by Eadon and Creighton, in their review of the ultraviolet/visible spectrum of 52 different metal nanospheres, in vacuum and in water.[22] Nowadays, the search for novel plasmonic candidates focuses on metallic alloys, (doped) semiconductors, and metamaterials.[23]

Measurable effects due to the plasmonic resonance include absorption and scattering, which are quantifiable by their cross sections. In the dipolar regime ($d \ll \lambda$), the Rayleigh formula for cross sections can be applied[15]

$$\sigma_{abs} = -k\mathrm{Im}[\alpha], \quad \sigma_{sca} = \frac{k^4}{6\pi}|\alpha|^2, \tag{19}$$

where k is the wave number. It is important to note the cross sections' dependence on α and, as a consequence, on the volume: since the absorption cross section σ_{abs} scales linearly with V while the scattering one σ_{sca} scales quadratically with it, it is reasonable to assume that smaller particles mainly absorb light while larger particles mainly scatter it.

However, the most prominent effect of plasmonic resonances is that of field enhancement. Outside the particle, the total field is a superposition of the incoming field $\vec{E}^0$ and of the dipolar field generated by the particle itself. For a continuous wave, the local field outside the nanoparticle takes the shape of a classical dipole field[24]

$$\vec{E}(\vec{r}) = \vec{E}^0 + \frac{1}{4\pi\epsilon_0\epsilon_h}\frac{3(\vec{r}\cdot\vec{p}_{np})\vec{r} - r^2\vec{p}_{np}}{r^5}, \tag{20}$$

where r is the distance from the center of the particle. As can be intuited, resonances in α will reflect on $\vec{p}_{np}$ and subsequently on $\vec{E}(\vec{r})$. Field enhancement is typically quantified by $|E|^2/|E^0|^2$ (as in Fig. 5). This factor can make the local electric field tens or hundreds of times higher than the incoming field. The shape of the particle can be engineered to create radiation enhancements that are wavelength-, polarization-, and direction-dependent, just like in classical antennas.[25,26]

One interesting effect can be noted in Fig. 5: along the direction orthogonal to the oscillation, the radiated field causes destructive interference with the incoming field, leading to areas where the field is quenched ($|E|^2/|E^0|^2 < 1$) instead of enhanced. This is possible because, in Eq. (20), for some $\vec{r}$ and at a certain frequency, $\vec{r}\cdot\vec{p}_{np} = 0$ and $|1 - (\alpha/4\pi r^3)|^2 < 1$.

The finite-difference time-domain simulations in Fig. 5 solve Maxwell's equations in discretized space and time, characterizing each portion of space with the complex dielectric function ϵ and complex magnetic permeability μ. These simulations introduce minimal approximations and accurately compute the electric and magnetic fields, presenting a case very close to reality. Using this simulation, the plasmonic resonance occurs at 540 nm, instead of 520 nm, as shown previously in Fig. 4. This shift is mainly explained as an effect of radiation damping,[27] which shows that the quasi-static approximation does not always provide accurate answers. This is why we need to look beyond it.

IV. BEYOND THE QUASI-STATIC APPROXIMATION

The quasi-static approximation describes nanoscale processes fairly well, such as the absorption of certain colors or the local field enhancement in the proximity of metal nanoparticles. However, it fails to predict other effects related to particle size: in the quasi-static approximation, particle size is irrelevant, as long as it is smaller than the incoming wavelength. Can we extend this theory to include the particle's size and shape?

The first correction we will introduce takes into account the collisions of the electrons with the nanoparticle boundaries, which have implicitly been neglected until now. Then,

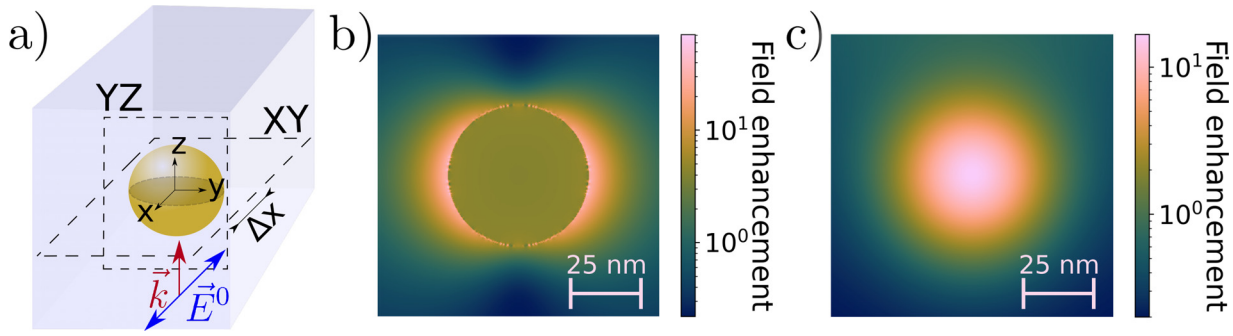

Fig. 5. Finite-difference time-domain (FDTD) simulation of the field enhancement at $\lambda = 540$ nm near a spherical gold nanoparticle of radius 25 nm in water. (a) Sketch of the simulated object, (b) field enhancement in the XY plane ($z = 0$), and (c) field enhancement in the YZ plane ($\Delta x = 4$ nm away from the surface of the nanoparticle). (The code for simulation in Lumerical's FDTD solutions can be found in the supplementary material and on GitHub (https://github.com/Brinkslab/LSP). The results were plotted in Spyder, using the color-vision deficiency friendly and perceptually uniform color map "batlow" (Ref. 42.)

the second correction will take us closer to the multipolar regime by involving retardation effects. Considering the classical nature of this extended model, it is impressive how well it fits experiments for such nanoscopic objects, as we will see.

A. Surface damping

Up to now, we have implicitly considered the damping frequency γ to be dominated by the collisions of electrons with other electrons, lattice nuclei or phonons. At a very small scale, however, electrons will also impact the particle boundary. This is notably the case when the dimensions of the particle are smaller than the mean free path, that is, the average distance traveled by the electron between two consecutive collisions. In other words, if the particle is small enough, the electrons will impact the boundary much more often than they collide with other objects.[15] The empirical model developed hereafter aims at taking this effect into account, and well matches experimental data. In the end, it is very similar to the exact one obtained via semiclassical calculations.[28,29]

As the free electrons move at the Fermi velocity v_F, the characteristic time between two consecutive collisions with the boundary will be

$$\tau_{boundary} = \frac{\lambda_{boundary}}{v_F}, \tag{21}$$

where $\lambda_{boundary}$ is the characteristic length of the process. By applying Matthiessen's rule (Eq. (2)), the damping frequency will become

$$\gamma = \gamma_{bulk} + \frac{1}{\tau_{boundary}} = \frac{v_F}{\lambda_{MFP}} + \frac{v_F}{\lambda_{boundary}}, \tag{22}$$

where γ_{bulk} is the bulk metal damping frequency and λ_{MFP} is the mean free path.

For a sphere of radius r, Kreibig[10] used the linear relation $\lambda_{boundary} = \frac{4}{3}r$, but coefficients between 1 and 4 have been used by other authors.[30–34] A simple and intuitive motivation for a coefficient of $\frac{4}{3}$ is provided hereafter, based solely on geometrical considerations.

Consider a spherical nanoparticle of radius r inside which electrons can travel only in straight trajectories. Let $O(x, y, z)$ be the initial point on the surface where an electron has just collided with the boundary, and let $O'(x', y', z')$ be a generic final point on the sphere surface where the electron will impact after traveling a distance $d[O, O']$. Then

$$x^2 + y^2 + z^2 = r^2, \quad x'^2 + y'^2 + z'^2 = r^2. \tag{23}$$

Since the scattering is assumed to be isotropic inside the sphere, all the points O' belonging to the surface have the same probability of being hit.

Without loss of generality, consider a reference system such that the initial point is $O(0, 0, r)$,

$$d[O, O'] = \sqrt{x'^2 + y'^2 + (z' - r)^2} = \sqrt{2}r\sqrt{1 - \frac{z'}{r}}. \tag{24}$$

The characteristic length of the process $\lambda_{boundary}$ can be defined as the average distance $d[O, O']$,

$$\lambda_{boundary} = \frac{\int_0^{2\pi}\int_{-r}^{r} d[O, O']dz'd\theta}{\int_0^{2\pi}\int_{-r}^{r} dz'd\theta} = \frac{\sqrt{2}\int_{-r}^{r}\sqrt{1 - \frac{z'}{r}}dz'}{2}. \tag{25}$$

By changing the integration variable

$$a = 1 - \frac{z'}{r} \Rightarrow dz' = -rda, \tag{26}$$

the integral can be rewritten and solved as follows:

$$\lambda_{boundary} = \frac{\sqrt{2}r}{2}\int_0^2 \sqrt{a}\, da = \frac{4}{3}r. \tag{27}$$

Now let us examine the consequences of surface damping. Around the plasma frequency, it is almost always true that $\omega \gg \gamma$ (refer to Table I for the realistic orders of magnitude), so in first approximation, the Drude model in Eq. (3) becomes

$$\epsilon_1 \approx \epsilon_{m,\infty} - \frac{\omega_P^2}{\omega^2}, \quad \epsilon_2 \approx \frac{\omega_P^2\gamma}{\omega^3}. \tag{28}$$

While the real part is almost unchanged when introducing the damping correction, near the resonance frequency (as defined by the Fröhlich condition in Eq. (18)), the imaginary part can be rewritten as

$$\epsilon_2 \approx \frac{\omega_P^2}{\omega_{res}^3}\left(\gamma_{bulk} + \frac{3v_F}{4r}\right) = \epsilon_{2_{bulk}} + A\frac{v_F}{r}, \tag{29}$$

where we have employed the Kreibig relation for spherical nanoparticles, and $A = 3/4(\omega_p^2/\omega_{res}^3)$. For very small particles this implies that, at ω_{res}, the condition of small ϵ_2 is not true anymore, therefore drastically diminishing the resonance peak in α. A calculated example for a nanoparticle with gold-like parameters in water is provided in Fig. 6(a) for various particle sizes.

B. Modified long-wavelength approximation

The dipolar approximation is valid as long as the dimensions of the metal nanoparticle are such that $d \ll \lambda$. Otherwise, variations in the incoming field will not be negligible, and multipolar modes will eventually be excited. Between this dipolar treatment and the brute-force computational solution of Maxwell's equations lies the so-called modified long-wavelength approximation (MLWA), a correction to the polarizability obtained in the quasi-static approximation (QSA) that includes retardation effects.[17]

The MLWA treats each atom in the nanoparticle as a dipole emitter and takes into account that its electric field propagates at the speed of light c (and not instantly), causing a retarded dipolar field. While in the QSA we imposed $\vec{k}\cdot\vec{r} = 0$ (Eq. (4)), in the following derivation of the MLWA equations, the dipole radiation is expanded in a Taylor series up to the third order $(kr)^3$. The infinitesimal electric field is integrated over the volume of the particle, and finally a corrected polarizability α_{MLWA} is defined.

Using the complex notation, an oscillating dipole moment p can be expressed as

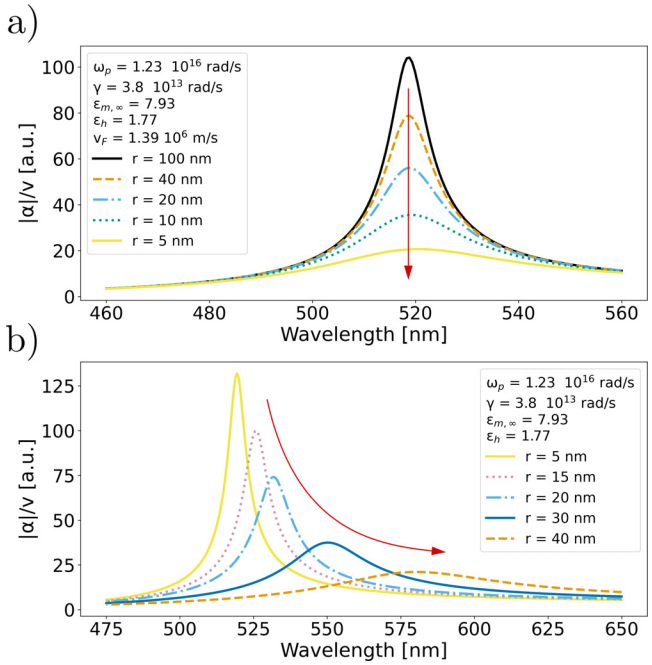

Fig. 6. Corrections to the quasi-static approximation: (a) Surface damping effect calculated from Eq. (29) and (b) modified long-wavelength approximation (MLWA) calculated from Eq. (38). The red arrows indicate the effects of either correction on peak positions and intensities, as a function of decreasing, respectively, increasing, particle radius. (Plot colors have been selected according to the color-vision deficiency friendly color cycle proposed by Okabe and Ito and made popular by Wong (Ref. 41).)

$$p = p_0 e^{i\omega t} e^{-ikr}, \quad \dot{p} = i\omega p, \quad \ddot{p} = -\omega^2 p. \tag{30}$$

For a point emitter, the radial and tangential fields in spherical coordinates are[35]

$$E_R = \frac{2\cos\theta}{4\pi\epsilon_0\epsilon_h}\left(\frac{p}{r^3} + \frac{\dot{p}}{cr^2}\right),$$
$$E_\theta = \frac{\sin\theta}{4\pi\epsilon_0\epsilon_h}\left(\frac{p}{r^3} + \frac{\dot{p}}{cr^2} + \frac{\ddot{p}}{c^2 r}\right). \tag{31}$$

Since the component of the electric field orthogonal to the applied field cancels out on integration over the nanosphere (as shown in the supplementary material[43]), we only need to quantify the parallel one. For a point emitter,

$$E_{//} = E_R\cos\theta - E_\theta\sin\theta$$
$$= \frac{p_0 e^{i\omega t} e^{-ikr}}{4\pi\epsilon_0\epsilon_h}\left[2\cos^2\theta\left(\frac{1}{r^3} + \frac{i\omega}{cr^2}\right)\right.$$
$$\left. - \sin^2\theta\left(\frac{1}{r^3} + \frac{i\omega}{cr^2} - \frac{\omega^2}{c^2 r}\right)\right]. \tag{32}$$

Expanding e^{-ikr} to the third order, rewriting $\sin^2\theta = 1 - \cos^2\theta$ and making $\omega = kc$ explicit

$$E_{//} = \frac{p_0 e^{i\omega t}}{4\pi\epsilon_0\epsilon_h}\left[\cos^2\theta\left(\frac{3}{r^3} + \frac{k^2}{2r}\right) - \left(\frac{1}{r^3} - \frac{k^2}{2r} + \frac{i2k^3}{3}\right)\right]$$
$$= \frac{p_0 e^{i\omega t}}{4\pi\epsilon_0\epsilon_h}\left[\frac{1}{r^3}(3\cos^2\theta - 1) + \frac{k^2}{2r}(\cos^2\theta + 1) - \frac{i2k^3}{3}\right]. \tag{33}$$

As an extension of the QSA, we can treat the nanoparticle as a single emitter with a radiated field E_{MLWA} being the superposition of all the dipole fields with respect to its center. A convenient reference system takes $\vec{r} \to -\vec{r}$ ($r \to r, \theta \to -\theta$, $\phi \to \phi$), meaning that every vector starts from a point emitter in the sphere and points to its center. This coordinate change does not influence the signs in the equation because of the symmetry in θ. Therefore, for every volume element $dV = r^2\sin\theta dr d\theta d\phi$ inside the sphere, we will have a radiated field

$$dE_{MLWA} = \frac{1}{4\pi\epsilon_0\epsilon_h}\left[\frac{1}{r^3}(3\cos^2\theta - 1)\right.$$
$$\left. + \frac{k^2}{2r}(\cos^2\theta + 1) - \frac{i2k^3}{3}\right]dp$$
$$= \frac{1}{4\pi\epsilon_0\epsilon_h}\left[\frac{1}{r^3}(3\cos^2\theta - 1)\right.$$
$$\left. + \frac{k^2}{2r}(\cos^2\theta + 1) - \frac{i2k^3}{3}\right]Pr^2\sin\theta dr d\theta d\phi. \tag{34}$$

We finally integrate dE_{MLWA} over the volume of the sphere of radius R and factor the volume out to obtain the total MLWA correction

$$E_{MLWA} = \frac{1}{4\pi\epsilon_0\epsilon_h}\frac{4\pi}{3}\left(k^2R^2 - i\frac{2}{3}k^3R^3\right)P$$
$$= \frac{1}{4\pi\epsilon_0\epsilon_h}\left(\frac{k^2}{R} - i\frac{2}{3}k^3\right)p_{np}. \tag{35}$$

This formula can be generalized for ellipsoidal nanoparticles of semiaxes $a_j, j = x, y, z$,[17]

$$E_{MLWA,j} = \frac{1}{4\pi\epsilon_0\epsilon_h}\left(\frac{k^2}{a_j} - i\frac{2}{3}k^3\right)p_{np,j}. \tag{36}$$

At this point, we only need to rewrite $\vec{p}_{np}$,

$$\vec{p}_{np} = \epsilon_0\epsilon_h\vec{\alpha}\,(\vec{E}^0 + \vec{E}_{MLWA}) = \epsilon_0\epsilon_h\vec{\alpha}_{\,MLWA}\vec{E}^0, \tag{37}$$

from which

$$\alpha_{MLWA,j} = \frac{\alpha_j}{1 - \frac{\alpha_j}{4\pi}\left(\frac{k^2}{a_j} - i\frac{2}{3}k^3\right)}. \tag{38}$$

For sufficiently small nanoparticles, we retrieve the QSA ($\alpha_{MLWA,j} \approx \alpha_j$), as expected. For relatively small yet finite volumes, the imaginary term proportional to k^3 can be neglected ($\alpha_{MLWA,j} \approx 4\pi\alpha_j/4\pi - \alpha_j k^2/a_j$). For larger volumes, the imaginary term dominates the denominator.

The term $\alpha_j(k^2/a_j)$ in Eq. (38) is called dynamic depolarization, because it is obtained in a dynamic calculation ($k > 0$), and its coefficient is real, corresponding to a change in the effective particle depolarization factor. Let us recall that α_j is proportional to particle volume ($\alpha_j \propto a_x a_y a_z$). As $(a_x a_y a_z/a_j k^2)$ increases, a more negative value of ϵ_1 is necessary to meet the resonance condition. At small but finite particle volumes, this effect enhances the plasmonic resonance; at larger volumes, it is responsible for the shift of the resonance peak.

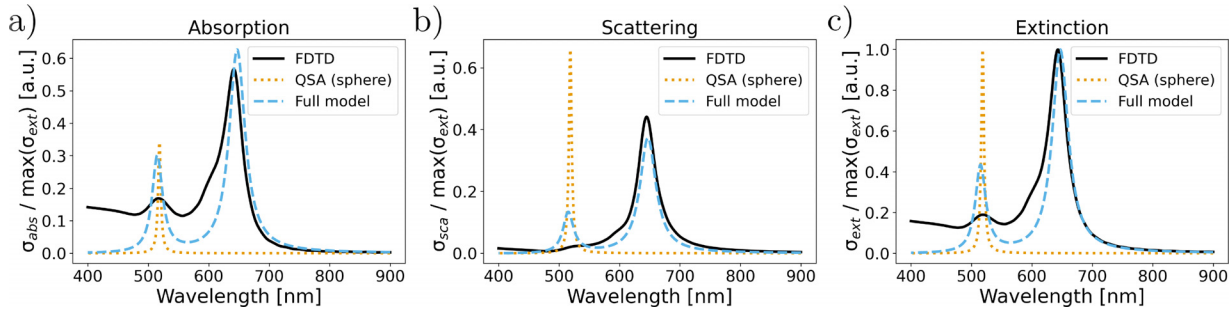

Fig. 7. (a) Absorption, (b) scattering, and (c) extinction cross sections for a gold ellipsoid immersed in water, having an aspect ratio $a_x/a_y = a_x/a_z = 2$ and a volume $v = \frac{4}{3}\pi(25\text{ nm})^3 = 6.54 \cdot 10^4\text{ nm}^3$. Comparison between a FDTD simulation, the quasi-static approximation of a gold-like sphere of the same volume, and the full analytical model for an ellipsoid. To account for both the longitudinal and transverse modes, cross sections have been calculated separately and averaged. The cross sections are each normalized to their own maximum extinction cross section, respectively. (Plot colors have been selected according to the color-vision deficiency friendly color cycle proposed by Okabe and Ito and made popular by Wong (Ref. 41).)

The term $-i\alpha_j\frac{2}{3}k^3$ in Eq. (38) is called radiative damping, because it arises from the spontaneous emission of radiation by the induced dipole. The term grows rapidly with particle volume. Being imaginary, it contributes heavily to ϵ_2 and, therefore, to the resonance damping. For relatively large particle volumes, it accounts for the damping by radiative losses and results in a broadening and a strong decrease in the plasmonic resonance (also counterbalancing the enhancement due to dynamic depolarization just mentioned).

According to this approximation, an increase in particle size (a_j) will result in a red-shifted, broadened and less intense plasmonic resonance. This is indeed what we notice in Fig. 6(b) in the calculated peaks for a nanoparticle with gold-like parameters immersed in water. The MLWA usually works well for nanoparticles of dimensions up to ≈200 nm,[36] above which multipolar resonances cannot be neglected, and computational methods are required.

The complete analytical model combines the corrected Drude model, the generalized Clausius–Mossotti formula for polarizability, the surface damping effect and the MLWA. In Fig. 7, an example for a gold elongated ellipsoid having $a_x/a_y = a_x/a_z = 2$ is presented against a gold sphere of $r = 25$ nm, of the same volume. The cross sections are calculated in the dipolar limit using Eq. (19). Agreement between the finite-difference time-domain (FDTD) simulation and the model is remarkable, both in the peak positions and the ratio of cross section components. Experimental evidence also corroborates this result.[37]

V. FINAL REMARKS

Starting from a general model for metals and from the polarization of a particle immersed in a dielectric host, we explored the effects of several features on the final resonance peak induced by an external oscillating electric field.

The analytical approach took us far into the understanding of the plasmonic resonance. However, as already hinted at the end of Sec. IV, the corrections to the quasi-static approximation have their own limitations. In fact, neglecting key features in the shape of the particle like spikes, neat edges, flat sides, or amorphous protrusions will result in incorrect predictions. Yet where the analytical approach fails, numerical simulations can be used. The most common numerical techniques include generalized Mie theory, finite-difference time-domain (FDTD), discrete dipole approximation (DDA), finite-element method (FEM), and boundary element method (BEM).[38,39] Each simulation technique has its own advantages and drawbacks.

Should this material be used as didactic reference, the authors strongly suggest the incorporation of at least some examples of applications from state-of-the-art research. These examples should be tailored depending on the interest of the course and can be directed towards optics, biophysics, or condensed matter physics. To learn more about light-matter interaction or expand knowledge about state-of-the-art plasmonics and emerging applications, the authors recommend Fox's[40] and Maier's[3] books, which provide valuable insight into the field and are very accessible for lecturers and students alike.

The properties of plasmonic resonances depend on material shape and intrinsic properties. The analytical approach supplied here is limited to ellipsoidal geometries but already takes into account virtually all relevant material properties (in a classical approximation). However, while only simulations will provide reliable descriptions of the plasmonic effects in realistic nanoparticles, the outlined fundamental approach, no matter its flaws, provides an understanding of why and how plasmonic resonances emerge in nanoparticles, and thus gives an intuitive basis and plausibility check for numerical design.

ACKNOWLEDGMENTS

D.B. acknowledges support by an ERC Starting Grant (No. 850818-MULTIVIsion), an NWO Start-up Grant (No. 740.018.018), and an NWO XS (No. CENW.XS2.033). M.L. thanks professors Maurizio Canepa and Francesco Bisio for inspiration.

AUTHOR DECLARATIONS

Conflict of Interest

The authors have no conflicts to disclose.

[a)]Electronic mail: m.locarno@tudelft.nl. ORCID: 0000-0002-7624-4859.
[b)]ORCID: 0000-0002-5550-5140.

[1]Bo Huang, Mark Bates, and Xiaowei Zhuang, "Super-resolution fluorescence microscopy," Annu. Rev. Biochem. **78**, 993–1016 (2009).
[2]Banqiu Wu and Ajay Kumar, "Extreme ultraviolet lithography: A review," J. Vacuum Sci. Technol. B **25**, 1743–1761 (2007).
[3]Stefan A. Maier, *Plasmonics: Fundamentals and Applications*, 1st ed. (Springer, Berlin, 2007).

[4]Robert W. Corkery and Eric C. Tyrode, "On the colour of wing scales in butterflies: Iridescence and preferred orientation of single gyroid photonic crystals," Interface Focus **7**, 28630678 (2017).
[5]Philippe Walter, Eléonore Welcomme, Philippe Hallégot, Nestor J. Zaluzec, Christopher Deeb, Jacques Castaing, Patrick Veyssière, René Bréniaux, Jean Luc Lévêque, and Georges Tsoucaris, "Early use of PbS nanotechnology for an ancient hair dyeing formula," Nano Lett. **6**, 2215–2219 (2006).
[6]Robert H. Brill and Nicholas D. Cahill, "A red opaque glass from sardis and some thoughts on red opaque in general," J. Glass Stud. **30**, 16–27 (1988), available at http://www.jstor.org/stable/24190804.
[7]David J. Barber and Ian C. Freestone, "An investigation of the origin of the colour of the Lycurgus cup by analytical transmission electron microscopy," Archaeometry **32**, 33–45 (1990).
[8]Mark L. Brongersma, "Introductory lecture: Nanoplasmonics," Faraday Discussions **178**, 9–36 (2015).
[9]Richard Gans, "Über die form ultramikroskopischer goldteilchen," Ann. Phys. **342**, 881–900 (1912).
[10]Uwe Kreibig, "Electronic properties of small silver particles: The optical constants and their temperature dependence," J. Phys. F: Met. Phys. **4**, 999–1014 (1974).
[11]Vincenzo Amendola, Roberto Pilot, Marco Frasconi, Onofrio M. Maragò, and Maria Antonia Iatì, "Surface plasmon resonance in gold nanoparticles: A review," J. Phys. Condens. Matter **29**, 203002 (2017).
[12]Andrés Guerrero-Martínez, Silvia Barbosa, Isabel Pastoriza-Santos, and Luis M. Liz-Marzán, "Nanostars shine bright for you. Colloidal synthesis, properties and applications of branched metallic nanoparticles," Curr. Opin. Colloid Interface Sci. **16**, 118–127 (2011).
[13]Suk Joo Youn, Tae Hwan Rho, Byung Il Min, and Kwang S. Kim, "Extended Drude model analysis of noble metals," Phys. Status Solidi (B) Basic Res. **244**, 1354–1362 (2007).
[14]David R. Lide, "Optical properties of selected elements," in *CRC Handbook of Chemistry and Physics*, 6th ed. (CRC Press (Internet version), Boca Raton, Florida, 2005).
[15]Craig F. Bohren and Donald R. Huffman, *Absorption and Scattering of Light by Small Particles* (John Wiley & Sons, New York, 1998).
[16]William L. Barnes, "Particle plasmons: Why shape matters," Am. J. Phys. **84**, 593–601 (2016).
[17]Lance K. Kelly, Eduardo Coronado, Lin Lin Zhao, and George C. Schatz, "The optical properties of metal nanoparticles: The influence of size, shape, and dielectric environment," J. Phys. Chem. B **107**, 668–677 (2003).
[18]Ming Li, Scott K. Cushing, and Nianqiang Wu, "Plasmon-enhanced optical sensors: A review," Analyst **140**, 386–406 (2015).
[19]Marek Piliarik, Pavel Kvasnička, Nicolle Galler, Joachim R. Krenn, and Jiří Homola, "Local refractive index sensitivity of plasmonic nanoparticles," Opt. Express **19**, 9213–9220 (2011).
[20]Stephan Link and Mostafa A. El-Sayed, "Spectral properties and relaxation dynamics of surface plasmon electronic oscillations in gold and silver nanodots and nanorods," J. Phys. Chem. B **103**, 8410–8426 (1999).
[21]Paul R. West, Satoshi Ishii, Gururaj V. Naik, Naresh K. Emani, Vladimir M. Shalaev, and Alexandra Boltasseva, "Searching for better plasmonic materials," Laser Photonics Rev. **4**, 795–808 (2010).
[22]J. Alan Creighton and Desmond G. Eadon, "Ultraviolet-visible absorption spectra of the colloidal metallic elements," J. Chem. Soc., Faraday Trans. **87**, 3881–3891 (1991).
[23]Alexandra Boltasseva and Harry A. Atwater, "Low-loss plasmonic metamaterials," Science **331**, 290–291 (2011).
[24]David J. Griffiths, *Introduction to Electrodynamics* (Cambridge U. P., Cambridge, 2017).
[25]Alberto G. Curto, Giorgio Volpe, Tim H. Taminiau, Mark P. Kreuzer, Romain Quidant, and Niek F. van Hulst, "Unidirectional emission of a quantum dot coupled to a nanoantenna," Science **329**, 930–933 (2010).
[26]Marta Castro-Lopez, Daan Brinks, and Niek F. van Hulst, "Non-reciprocal optical antennas," preprint arXiv:1412.4797 (2014).
[27]Benjamin M. Ross, Savas Tasoglu, and Luke P. Lee, "Plasmon resonance differences between the near- and far-field and implications for molecular detection," Proc. SPIE **7394**, 739422 (2009).
[28]Niels Asger Mortensen, Søren Raza, Martijn Wubs, Thomas Søndergaard, and Sergey I. Bozhevolnyi, "A generalized non-local optical response theory for plasmonic nanostructures," Nat. Commun. **5**, 3809–3815 (2014).
[29]Somayeh Karimi, Ahmad Moshaii, Sara Abbasian, and Maryam Nikkhah, "Surface plasmon resonance in small gold nanoparticles: Introducing a size-dependent plasma frequency for nanoparticles in quantum regime," Plasmonics **14**, 851–860 (2019).
[30]Asef Kheirandish, Nasser Sepehri Javan, and Hosein Mohammadzadeh, "Modified Drude model for small gold nanoparticles surface plasmon resonance based on the role of classical confinement," Sci. Rep. **10**, 6517 (2020).
[31]Cecilia Noguez, "Surface plasmons on metal nanoparticles: The influence of shape and physical environment," J. Phys. Chem. C **111**, 3806–3819 (2007).
[32]Kin Hung Fung and Che Ting Chan, "A computational study of the optical response of strongly coupled metal nanoparticle chains," Opt. Commun. **281**, 855–864 (2008).
[33]Eduardo A. Coronado and George C. Schatz, "Surface plasmon broadening for arbitrary shape nanoparticles: A geometrical probability approach," J. Chem. Phys. **119**, 3926–3934 (2003).
[34]Stéphane Berciaud, Laurent Cognet, Philippe Tamarat, and Brahim Lounis, "Observation of intrinsic size effects in the optical response of individual gold nanoparticles," Nano Lett. **5**, 515–518 (2005).
[35]Max Born and Emil Wolf, *Principles of Optics*, 7th ed. (Cambridge U. P., Cambridge, 2019).
[36]Ellen J. Zeman and George C. Schatz, "An accurate electromagnetic theory study of surface enhancement factors for Ag, Au, Cu, Li, Na, Al, Ga, In, Zn, and Cd," J. Phys. Chem. **91**, 634–643 (1987).
[37]Ming Zhang Wei, Tian Song Deng, Qi Zhang, Zhiqun Cheng, and Shiqi Li, "Seed-mediated synthesis of gold nanorods at low concentrations of CTAB," ACS Omega **6**, 9188–9195 (2021).
[38]James Parsons, Christopher P. Burrows, John R. Sambles, and William L. Barnes, "A comparison of techniques used to simulate the scattering of electromagnetic radiation by metallic nanostructures," J. Mod. Opt. **57**, 356–365 (2010).
[39]Manuel R. Gonçalves, "Plasmonic nanoparticles: Fabrication, simulation and experiments," J. Phys. D: Appl. Phys. **47**, 213001 (2014).
[40]Mark Fox, *Optical Properties of Solids*, 2nd ed. (Oxford U. P., Oxford, 2010).
[41]Bang Wong, "Points of view: Color blindness," Nat. Methods **8**, 441 (2011).
[42]Fabio Crameri, Grace E. Shephard, and Philip J. Heron, "The misuse of colour in science communication," Nat. Commun. **11**, 5444 (2020).
[43]See supplementary material at https://www.scitation.org/doi/suppl/10.1119/5.0094967 for additional information on light-matter interaction, the derivation of the Lorentz oscillator, the conversion of the Lorentz oscillator to the Drude model for metals, skin depth considerations, normalization of depolarization factors, the orthogonal component of the electric field in the MLWA, signs and conventions, and details about Lumerical's FDTD Solutions and Python code to reproduce and plot the simulations.